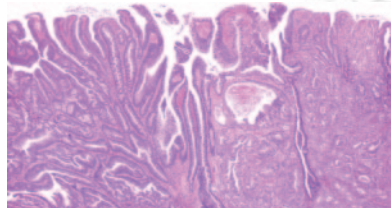


**Weissberg** outlines the importance of underlying cell biology in understanding the potential for nuclear medicine imaging of atherosclerotic plaques. . . . *Page 1794*

**Kumar and colleagues** assess the predictive value of positive  $^{18}\text{F}$ -FDG PET findings after completion of chemotherapy in patients with gastrointestinal lymphomas and compare the ability of PET and CT to detect residual disease. . . . *Page 1796*

**Kamel and colleagues** report on the significance of incidentally detected gastrointestinal tract lesions and the effects of early identification on patient management and outcomes in a large screening population. . . . *Page 1804*



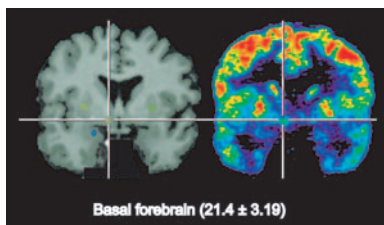
**Heiss and colleagues** evaluate the applications of a new scanner with improved spatial resolution that permits the determination of metabolic rates in small nuclei associated with various neurodegenerative disorders. . . . *Page 1811*

**Ben-Haim and colleagues** report on the ability of PET/CT to identify and localize focal vascular-wall  $^{18}\text{F}$ -FDG uptake and discuss the potential for early detection of patients at increased risk of future cardiovascular events. . . . *Page 1816*

**Tiling and colleagues** investigate whether tissue-specific parameters—in addition to lesion size—may affect uptake of  $^{99\text{m}}\text{Tc}$ -sestamibi in scintimammography. . . . *Page 1822*

**Tseng and colleagues** assess the ability of PET to characterize biologic re-

sponse of locally advanced breast cancer to chemotherapy using  $^{15}\text{O}$ -water-derived blood flow measurements and  $^{18}\text{F}$ -FDG-derived glucose metabolism rate parameters. . . . *Page 1829*



**Yamane and colleagues** look at changes in  $^{18}\text{F}$ -FDG uptake on PET as early as 1 day after initiation of chemotherapy in patients with malignant lymphoma and discuss the implications that these changes have for accurate diagnosis and staging. . . . *Page 1838*

**Choi and colleagues** identify the predictive elements that contribute to the success of  $^{18}\text{F}$ -FDG PET in providing noninvasively independent prognostic information in preoperative esophageal squamous cell carcinoma. . . *Page 1843*

**Bruehlmeier and colleagues** discuss the use of late  $^{18}\text{F}$ -FMISO PET in providing a spatial description of hypoxia in brain tumors, independent of blood-brain barrier disruption and tumor perfusion. . . . *Page 1851*

**Chiu and colleagues** study patients with Alzheimer's disease and evaluate results suggesting a relationship between education level and differences in regional cerebral flow as measured by  $^{99\text{m}}\text{Tc}$ -HMPAO SPECT. . . . *Page 1860*

**Love and colleagues** compare coincidence detection-based  $^{18}\text{F}$ -FDG PET imaging with combined  $^{111}\text{In}$ -labeled leuko-

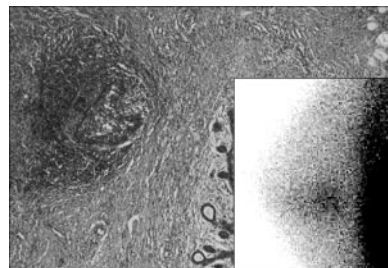
cyte/ $^{99\text{m}}\text{Tc}$ -sulfur colloid marrow imaging in the diagnosis of infection in patients with failed prosthetic joints. . . . *Page 1864*

**Krishnamurthy and colleagues** detail the results of a long-term study on the constancy and variability of gallbladder ejection fraction in conditions such as chronic calculus cholecystitis and chronic acalculous cholecystitis. . . . *Page 1872*

**Kasama and colleagues** assess whether dobutamine stress  $^{99\text{m}}\text{Tc}$ -tetrofosmin quantitative gated SPECT can be used to predict improvement of cardiac function and heart failure symptoms in patients receiving carvedilol therapy for idiopathic dilated cardiomyopathy. . . . *Page 1878*

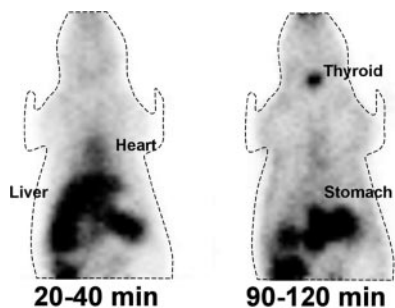
**Yoshinaga and colleagues** use  $^{11}\text{C}$ -acetate PET to investigate differences in oxidative metabolic response in myocardium and discuss the implications of these findings for the interpretation of  $^{18}\text{F}$ -FDG PET cardiac images. . . . *Page 1885*

**Wong and colleagues** research the feasibility of using  $^{18}\text{F}$ -FDG PET to quantify reduction of hepatic tumor metabolism after  $^{90}\text{Y}$ -glass microsphere treatment for unresectable metastatic disease to the liver. . . . *Page 1892*



**Davies and colleagues** review the biology of atherosclerosis, conventional imaging techniques, and the potential of nu-

clear imaging to provide valuable information on the cellular, metabolic, and molecular composition of plaque. . . . . **Page 1898**



**Katoh and colleagues** describe and illustrate the application of an algorithm that allows stable, rapid, and automated quantification of regional myocardial blood flow with  $^{15}\text{O}$ -water PET. . . **Page 1908**

**Miyagawa and colleagues** compare 2 herpes simplex virus reporter gene expres-

sion approaches for use in PET monitoring of gene therapy in rat and pig models. . . . . **Page 1917**

**Croteau and colleagues** use small-animal PET to evaluate the effects of 2 anesthetic agents on myocardial perfusion and coronary reserve in rats under rest and stress conditions. . . . . **Page 1924**

**Spaeth and colleagues** report on animal experiments designed to assess the potential of  $^{18}\text{F}$ -FET and  $^{18}\text{F}$ -FCH as PET tracers in differentiating radiation necrosis from tumor recurrence. . . . **Page 1931**

**van Waarde and colleagues** evaluate the in vitro and in vivo characteristics of 2 novel radioligands and discuss their potential for tumor detection and assessment of the  $\sigma$ -receptor occupancy of novel therapeutic drugs. . . . . **Page 1939**

**Murakami and colleagues** report on a study designed to measure brain concentrations of an  $^{11}\text{C}$ -labeled immunosuppressive agent in monkeys and outline possible applications in PET imaging of stroke. . . . . **Page 1946**

**Marshall and colleagues** investigate the accuracy of  $^{18}\text{F}$ -fluorodihydroroteronone as a deposited myocardial flow tracer and compare the results from investigations in the rabbit heart with those for  $^{201}\text{Tl}$ . . . . . **Page 1950**

**Hindorf and colleagues** evaluate the influence of the mass, shape, and distances between organs on S values in radionuclide studies of mice. . . . . **Page 1960**

**Zanzonico and colleagues** derive estimates of normal-tissue absorbed doses for  $^{18}\text{F}$ -FDHT PET imaging in patients with advanced prostate cancer. . . . . **Page 1966**

## ON THE COVER

Visual comparison of  $^{15}\text{O}$ - $\text{H}_2\text{O}$  PET perfusion images and late  $^{18}\text{F}$ -fluoromisonidazole (FMISO) PET images of patients with glioblastoma showed a large range of tumor perfusion within areas of increased  $^{18}\text{F}$ -FMISO uptake (i.e., hypoxia was present in both hypoperfused and hyperperfused tumor areas). Generally, increased  $^{18}\text{F}$ -FMISO uptake was found in the tumor margin but not in the tumor center. Tumor centers of all glioblastomas showed decreased radioactivity in both  $^{15}\text{O}$ - $\text{H}_2\text{O}$  and  $^{18}\text{F}$ -FMISO PET images. The perfusion-hypoxia patterns suggested that hypoxia in these tumors may develop irrespective of the magnitude of perfusion.

